Topographic and Tomographic Properties of Forme Fruste Keratoconus Corneas

Alain Saad[1,2] *and Damien Gatinel*[1,2]

Purpose. To investigate the efficacy of topography and tomography indices combined in discriminant functions to detect mild ectatic corneas.

Methods. The authors retrospectively reviewed the data of 143 eyes separated into three groups by the Corneal Navigator OPD scanning system (Nidek, Gamagori, Japan): normal (N; LASIK surgery with a 2-year follow-up; $n = 72$), forme fruste keratoconus (N topography with contralateral KC; FFKC; $n = 40$), and KC ($n = 31$). Topography and tomography indices, corneal thickness spatial profile (CTSP), and anterior and posterior curvature spatial profiles were obtained with the Orbscan IIz (Bausch & Lomb Surgical, Rochester, NY). The percentage of thickness increase (PTI) from the thinnest point to the periphery, the percentage of variation of anterior (PVAK), and posterior curvature were calculated and compared by Kruskal-Wallis test. The usefulness of these data to discriminate among the three groups was assessed by receiver operating characteristic (ROC) curve analysis.

Results. Posterior elevation of the thinnest point (TP), all positions of CTSP, PTI for all distances from the TP, and PVAK from a 5- to 7-mm distance from the TP were significantly different in the FFKC compared with the N group. The discriminant functions between the FFKC and the N groups and between the KC and the N groups reached an area under the ROC curve of 0.98 and 0.99, respectively. PTI indices and maximum posterior central elevation were the most important contributors to the discriminant function.

Conclusions. Indices generated from corneal thickness and curvature measurements over the entire cornea centered on the TP can identify very mild forms of ectasia undetected by a Placido-based neural network program. (*Invest Ophthalmol Vis Sci.* 2010;51:5546–5555) DOI:10.1167/iovs.10-5369

There has been a great interest in attempting to identify patients at risk for post-LASIK corneal ectasia before surgery. It is now known that corneas that share similarities with ectatic corneas (keratoconus or pellucid marginal corneal degeneration) are at higher risk for this complication.[1–4] Thus, efforts have been concentrated on using available specular topography, tomography, or biomechanical studies to recognize keratoconus (KC) in its earliest stages.[5–12] KC is a noninflammatory progressive localized thinning and protrusion of the cornea. The progressive nature of the disease makes it easily recognized in its advanced stages. However, there is a persistent ambiguity regarding the exact definition of a suspect keratoconus (KCS) cornea, and there are no widely accepted criteria for categorizing an eye as KCS.[13–15] It has been debated whether the first detectable sign of KC, consequently defining the KCS category, is a localized steepening seen with Placido corneal topography[15–19] or a slight bowing of the posterior corneal surface detected by tomography.[9,14,20] Current biomechanical parameter (corneal hysteresis and corneal resistance factor) studies have shown that KCS corneas differ significantly from normal and KC corneas, but the results have been of little clinical value until now.[5] An important practical task for clinicians is to improve the sensitivity of their screening methods for identifying patients with mild manifestations of KC and prevent iatrogenic keratectasia. Even if only one eye is affected initially, KC is an asymmetric progressive disorder that will ultimately affect both eyes. The reported frequency of unilateral KC among all KC patients varies, depending on the methods used for diagnosis. The estimated prevalence of unilateral KC ranges from 14.3% to 41% in studies in which only clinical parameters were considered.[21–23] In more recent studies, the reported frequencies based on computerized videokeratography diagnostic techniques ranged from 0.5% to 4%.[18,24] Thus, the incidence of true unilateral KC is very low, and results in some studies have suggested that, if patients are observed for a sufficient period, signs of keratoconus will develop in the opposite eye.[23,24] This conclusion was reached mainly because both eyes in unilateral KC have the same genetic makeup, and therefore the less-affected eye is also thought to have KC,[15] considering that KC is genetically described as a model of autosomal dominant transmission with complete penetrance but incomplete expression.[25–28] Therefore, the term forme fruste KC (FFKC), first proposed by Amsler in 1961[29] and then adopted by Klyce et al.,[15] should be used to define the contralateral eye in unilateral KC, the forme fruste being "an incomplete, abortive, or unusual form of a syndrome or disease."[29]

Thus, investigating these particular eyes and determining the topographic and tomographic characteristics of their corneas may help to identify at-risk corneas.

The purposes of our study were to describe and compare topography and tomography indices, as well as the central to periphery percentage of thickness increase and the percentage of anterior and posterior curvature modification in three groups of corneas classified as normal (N; LASIK with a 2-years follow-up), FFKC, and KC by specular topography, on the basis of the artificial intelligence of the Corneal Navigator OPD system (Nidek Co., Ltd., Gamagori, Japan)[30–32] and then to combine those indices in discriminant functions to detect mild ectatic corneas.

Methods

This retrospective study adhered to the tenets of the Declaration of Helsinki and included 143 eyes of 143 patients divided into three groups: normal, FFKC, and KC. Only one eye of each patient was included.

The Orbscan IIz (Bausch & Lomb Surgical, Rochester, NY) and OPD-Scan (Corneal Navigator; Nidek Co., Ltd.) videokeratographs were ob-

From the [1]Rothschild Foundation, Paris, France; and the [2]Center for Expertise and Research in Optics for Clinicians (CEROC), Paris, France.

Submitted for publication February 11, 2010; revised March 29, April 30, and June 1, 2010; accepted June 9, 2010.

Disclosure: **A. Saad**, None; **D. Gatinel**, None

Corresponding author: Damien Gatinel, Fondation Ophtalmologique Adolphe de Rothschild, 25, Rue Manin, 75019, Paris, France; gatinel@aol.com.

tained by two experienced operators. Segregation of the three groups was based on the results of the Nidek Corneal Navigator (NCN), which uses an artificial intelligence technique to train a computer neural network to recognize specific classifications of corneal topography. The NCN first calculates various indices representing corneal shape characteristics. The indices are then used by the NCN to score the measurement's similarity to nine clinical classification types: normal, astigmatism, suspected keratoconus, keratoconus, pellucid marginal degeneration, postkeratoplasty, myopic refractive surgery, hyperopic refractive surgery, and unclassified variation. These diagnostic results are estimated based on the relationship between the corneal indices and cases. The percentage of similarity is indicated for each diagnostic condition; the value varies from 0% to 99%. The indicated result for each topography condition is independent from other categories.

Eyes in the normal group had a score of 99% similarity to normality using the NCN analysis. In addition, data provided by the Orbscan IIz (Bausch & Lomb Surgical, Inc.) for the normal group did not reveal any topography patterns suggestive of KCS, such as focal or inferior steepening of the cornea or central keratometry greater than 47.0 D. This group was composed of 72 eyes surgically treated with LASIK with a 2-year follow-up, in which no complications such as ectasia were observed. The FFKC group was composed of 40 contralateral eyes of KC cases (Figs. 1, 2). The NCN analysis indicated a null score similarity to KCS and KC for the selected eyes and a nonnull score similarity to KC for the contralateral eyes (Fig. 2). The contralateral eyes also had a frank KC aspect on the curvature topography. The keratoconus group included 31 eyes that had frank keratoconus diagnosed by an experienced corneal specialist on the basis of clinical and topographic signs (with a positive similarity score to KC indicated by the NCN).

Orbscan IIz is a three-dimensional slit-scanning topography system used for analysis of the corneal anterior and posterior surfaces as well as pachymetry. It uses a slit-scanning system to measure 18,000 data points and a Placido-based system to make necessary adjustments to produce topography data.

On the Orbscan IIz, elevation maps are plotted by default against a spherical reference surface whose radius and position are calculated

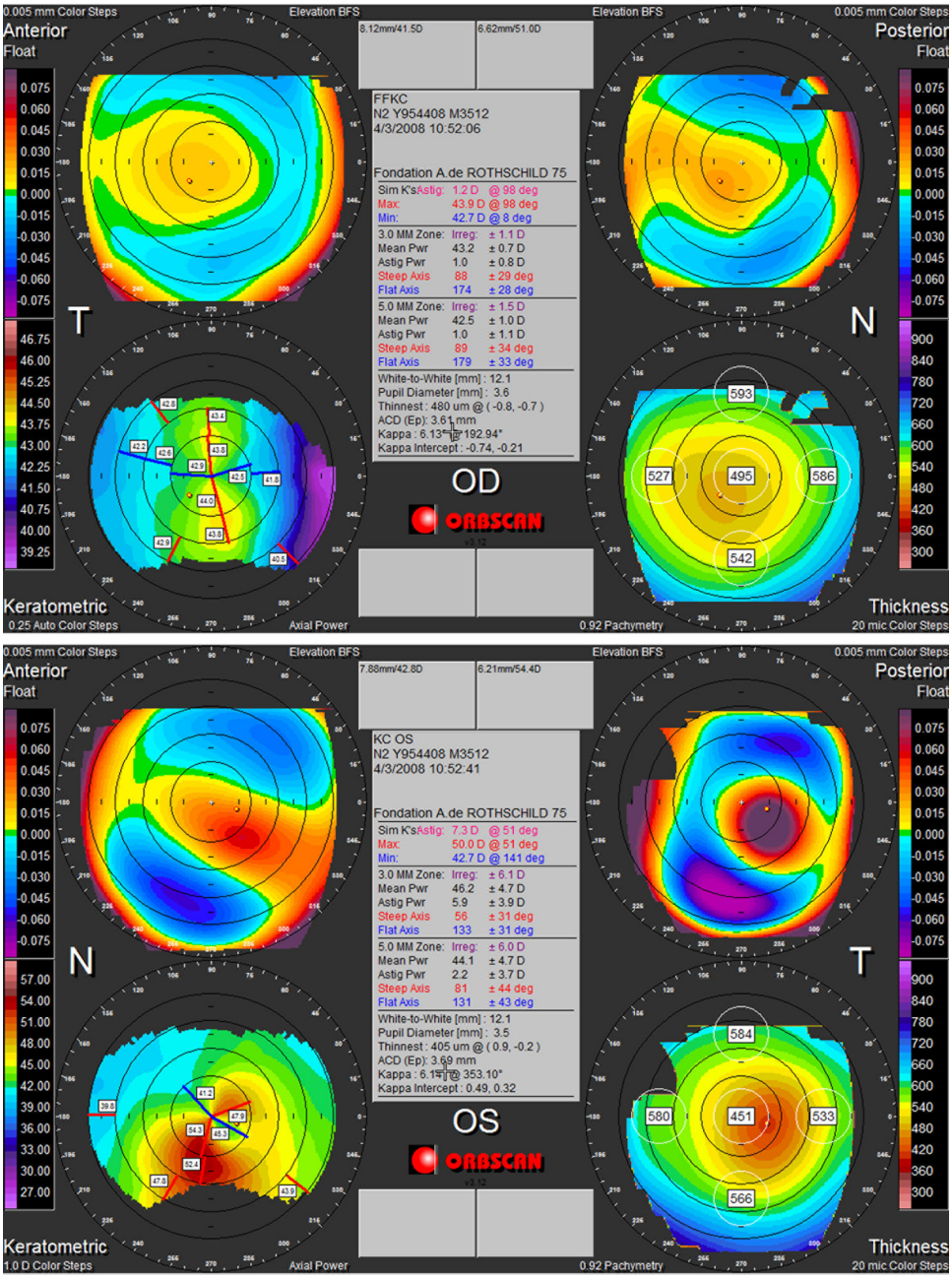

FIGURE 1. Orbscan IIz Quad Map of a FFKC (OD) and the contralateral KC (OS).

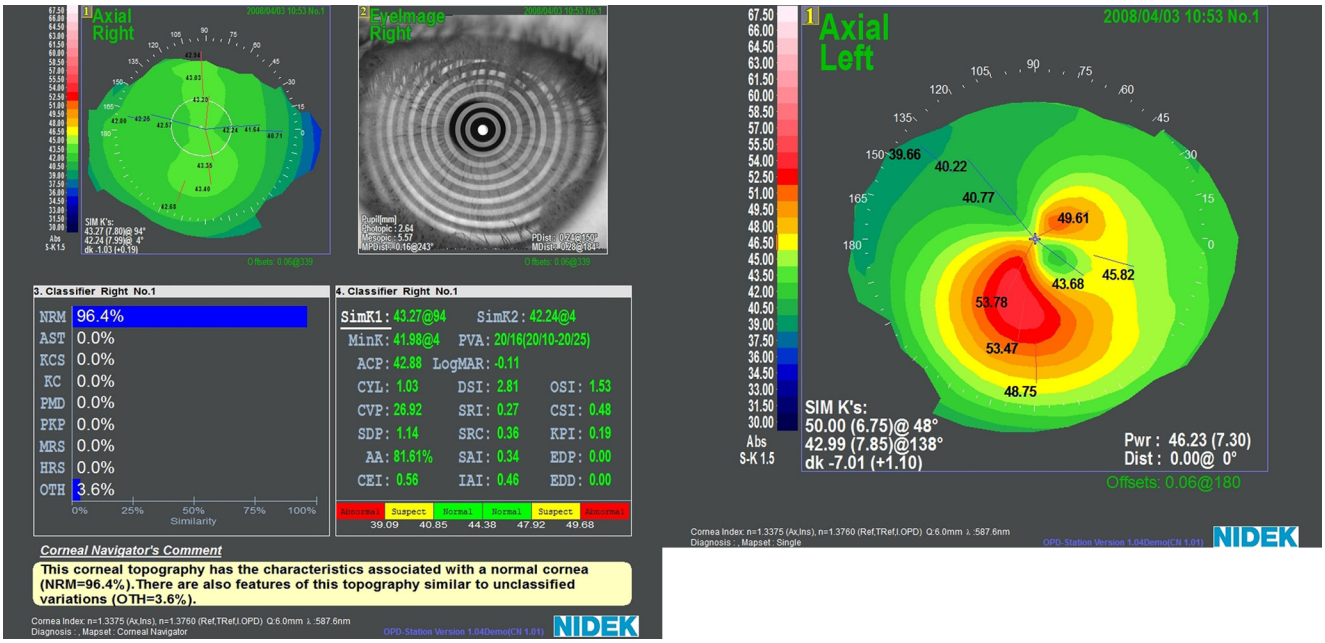

Figure 2. OPD scan and NCN of the FFKC (OD) described in Figure 1 and the contralateral KC.

without constraints (float mode). The following criteria were analyzed and compared by using the Orbscan Quad Map representation: central power and radius in both anterior best-fit sphere (BFS) and posterior BFS; maximum anterior central elevation (MACE) and posterior central elevation (MPCE) relative to the BFS in the central 1.0-mm radius zone; simulated keratometry in maximum (SK_{max}) and minimum (SK_{min}) dioptric values; irregularity index at 3.0 and 5.0 mm; central pachymetry (CP); thinnest pachymetry (TP); and magnitude of the decentration of the thinnest corneal point from the corneal geometric center (DTP). All values except MACE and MPCE are directly available from the Quad Map display mode. The MACE and MPCE values can be obtained via the Stats menu, which is accessed through the Tools menu on the main toolbar. The elevation and topography and tomography maps can be rotated to view the acquired image in a different perspective. This positioning is accomplished by determining the perpendicular to the surface at the specified center location. The surface is then rotated to bring the new center to the map center and the surface normal parallel to the instrument axis. The rotation is obtained via the Tools menu, by clicking on the surface rotation button and selecting the preferred center location. We considered the TP of the cornea as the center location to obtain the following data:

The elevation of the TP (AETP and PETP: anterior and posterior elevation of the TP), acquired by manually guiding the cursor over the center of the anterior and posterior elevation maps, respectively.

The anterior and posterior averages of keratometry values of the points on nine circular adjacent rings of 0.5-mm width centered on the TP. These keratometry values were processed from the slit scanning data rotated and centered on the TP. The outer diameter of each ring varied from 1 mm (inner ring) to 9 mm (outer ring). Knowing the mean keratometry of each ring, we calculated the anterior and posterior central to peripheral percentage of variation in anterior and posterior curvature (increase or decrease; PVAK_n, and PVPK_n) for each radius with the formula: PVA(P)K_n = [K_n − ($K_{n-0.5}$)]/$K_{n-0.5}$ where K_n is the mean corneal curvature at each radius and n represents the radius of imaginary rings centered on the TP. In contrast to asphericity, which is a global descriptor of the rate of change of curvature between the center and the periphery of the cornea, the PVA(P)K represents the local variation in the curvature with steps of 0.5 mm of radius. Therefore, it provides a more exhaustive and complete approach to investigating the changes in corneal curvature in the studied population. Similarly, the averages of thickness values of the points located on nine rings centered on the TP were obtained to create the corneal thickness profile. We calculated the percentage of thickness increase[33,34] for each ring (PTI), using the following formula: PTI = (T_n − TP)/TP where T_n is the corneal thickness average at each rings and n represents the radius of the outer perimeter of each ring centered on the TP.

All numerical results were entered into a database, and statistical analyses were performed (xLSTAT2009 statistical analysis software; Addinsoft, New York, NY) with the Kruskal-Wallis test followed by a Dunn procedure for multiple nonparametric comparisons and a Bonferroni correction to maintain a global level of $P < 0.05$.

Discriminant analysis was used to determine the group of an observation based on a set of variables obtained from the anterior and posterior corneal surface and from the thickness spatial profile. On the basis of the N and FFKC groups, the discriminant analysis

Table 1. Demographic Characteristics of Patients

Characteristics	Normal	FFKC	KC
Patients, *n*	72	40	31
OD, *n* (%)	44 (61)	20 (50)	16 (52)
Mean age, y ± SD	33.3 ± 9.3	33.4 ± 13.1	32.0 ± 7.7
Male sex, *n* (%)	24 (33)	27 (67)	24 (77)
Mean SE, D (range)	−4.16 ± 2.77 (−11.00 to −0.50)	−1.13 ± 0.96 (−2.50 to 0.50)	−7.74 ± 3.14 (−15.75 to 0.00)

SE, spherical equivalent.

constructs a set of linear functions of the variables, known as discriminant functions, such as

$$L = b_1x_1 + b_2x_2 + b_nx_n + c$$

where b is a discriminant coefficient, x is an input variable, and c is a constant. The following discriminant functions were generated:

FT: elevation and decentration of the TP

FPTI: percentage of thickness increase over the entire cornea

FPVAK: percentage of variation of anterior curvature over the entire cornea

FPVPK: percentage of variation of posterior curvature over the entire cornea

TABLE 2. All Studied Factors and Intergroup Comparison

	Mean ± SD			Kruskal-Wallis and Dunn Procedure		
	N	**FFKC**	**KC**	**N vs. FFKC**	**N vs. KC**	**KC vs. FFKC**
n	72	40	31			
Anterior BFS, D	42.5 ± 1.1	42.24 ± 1.44	43.64 ± 1.77	>0.05	**0.001**	**0.001**
Posterior BFS, D	51.6 ± 1.8	51.36 ± 2.26	54.01 ± 2.74	>0.05	**<0.0001**	**<0.0001**
Max sim K, D	43.9 ± 1.2	43.69 ± 1.60	48.37 ± 4.20	>0.05	**<0.0001**	**<0.0001**
Min sim K, D	43.1 ± 1.2	42.8 ± 1.6	45.2 ± 3.4	>0.05	**0.002**	**0.002**
Irreg 3 mm, D	0.98 ± 0.34	1.25 ± 0.38	5.01 ± 2.47	**<0.0001**	**<0.0001**	**<0.0001**
Irreg 5 mm, D	1.3 ± 0.3	1.64 ± 0.42	4.98 ± 2.35	**<0.0001**	**<0.0001**	**<0.0001**
Central pachymetry, μm	554.6 ± 36.1	524.3 ± 37.0	487.5 ± 52.1	**<0.0001**	**<0.0001**	**<0.0001**
Thinnest pachymetry, μm	547.8 ± 36.3	512.2 ± 37.6	464.2 ± 55.0	**<0.0001**	**<0.0001**	**<0.0001**
Difference CP - TP	6.8 ± 3.1	12.1 ± 5.6	23.3 ± 14.3	**<0.0001**	**<0.0001**	**<0.0001**
Decentration TP*x*	0.33 ± 0.47	0.49 ± 0.59	0.67 ± 0.31	>0.05	**0.002**	>0.05
Decentration TP*y*	−0.22 ± 0.36	−0.47 ± 0.50	−0.51 ± 0.47	**<0.001**	**<0.001**	>0.05
Decentration TP $[\sqrt{(TPx)^2 + (TPy)^2}]$	0.64 ± 0.32	0.95 ± 0.37	0.96 ± 0.30	**<0.0001**	**<0.0001**	>0.05
MACE	10.6 ± 3.6	12.6 ± 4.2	42.1 ± 21.2	>0.05	**<0.0001**	**<0.0001**
MPCE	21.9 ± 7.9	27.2 ± 11.2	79.0 ± 38.8	>0.05	**<0.0001**	**<0.0001**
AETP	7.4 ± 3.5	9.3 ± 3.8	33.0 ± 23.5	>0.05	**<0.0001**	**<0.0001**
PETP	19.7 ± 8.6	26.3 ± 11.0	73.2 ± 37.5	**<0.0001**	**<0.0001**	**<0.0001**
Anterior curvature						
1 mm	43.29 ± 1.47	43.47 ± 1.55	50.46 ± 6.40	>0.05	**<0.0001**	**<0.0001**
2 mm	43.36 ± 1.36	43.52 ± 1.46	50.13 ± 5.82	>0.05	**<0.0001**	**<0.0001**
3 mm	43.44 ± 1.23	43.53 ± 1.36	49.13 ± 4.72	>0.05	**<0.0001**	**<0.0001**
4 mm	43.43 ± 1.19	43.43 ± 1.36	47.73 ± 3.70	>0.05	**<0.0001**	**<0.0001**
5 mm	43.32 ± 1.18	43.24 ± 1.39	46.26 ± 2.90	>0.05	**<0.0001**	**<0.0001**
6 mm	43.14 ± 1.16	42.96 ± 1.39	44.99 ± 2.32	>0.05	**<0.0001**	**<0.0001**
7 mm	42.84 ± 1.13	42.58 ± 1.39	43.98 ± 1.93	>0.05	**0.002**	**0.002**
8 mm	42.46 ± 1.07	42.17 ± 1.39	43.17 ± 1.75	>0.05	>0.05	**0.014**
9 mm	42.00 ± 1.05	41.72 ± 1.48	42.49 ± 1.57	>0.05	>0.05	**0.032**
Pachymetry						
1 mm	0.549 ± 0.036	0.515 ± 0.035	0.467 ± 0.054	**<0.0001**	**<0.0001**	**<0.0001**
2 mm	0.554 ± 0.036	0.520 ± 0.035	0.476 ± 0.053	**<0.0001**	**<0.0001**	**<0.0001**
3 mm	0.563 ± 0.035	0.531 ± 0.035	0.494 ± 0.050	**<0.0001**	**<0.0001**	**<0.0001**
4 mm	0.575 ± 0.035	0.546 ± 0.034	0.518 ± 0.048	**<0.0001**	**<0.0001**	>0.05
5 mm	0.591 ± 0.035	0.563 ± 0.034	0.546 ± 0.046	**<0.0001**	**<0.0001**	>0.05
6 mm	0.611 ± 0.035	0.583 ± 0.034	0.575 ± 0.044	**<0.0001**	**<0.0001**	>0.05
7 mm	0.632 ± 0.036	0.604 ± 0.035	0.602 ± 0.041	**<0.0001**	**<0.0001**	>0.05
8 mm	0.656 ± 0.038	0.627 ± 0.036	0.628 ± 0.040	**<0.0001**	**<0.0001**	>0.05
9 mm	0.673 ± 0.040	0.646 ± 0.038	0.646 ± 0.039	**<0.0001**	**<0.0001**	>0.05
Posterior curvature						
1 mm	−6.17 ± 0.46	−6.05 ± 0.78	−7.69 ± 1.23	>0.05	**<0.0001**	**<0.0001**
2 mm	−6.50 ± 0.25	−6.64 ± 0.39	−8.22 ± 1.10	>0.05	**<0.0001**	**<0.0001**
3 mm	−6.44 ± 0.23	−6.54 ± 0.33	−7.83 ± 0.89	>0.05	**<0.0001**	**<0.0001**
4 mm	−6.38 ± 0.22	−6.43 ± 0.29	−7.39 ± 0.67	>0.05	**<0.0001**	**<0.0001**
5 mm	−6.32 ± 0.21	−6.32 ± 0.26	−6.96 ± 0.49	>0.05	**<0.0001**	**<0.0001**
6 mm	−6.23 ± 0.21	−6.20 ± 0.26	−6.58 ± 0.36	>0.05	**<0.0001**	**<0.0001**
7 mm	−6.13 ± 0.22	−6.10 ± 0.29	−6.27 ± 0.32	>0.05	>0.05	>0.05
8 mm	−6.03 ± 0.24	−6.04 ± 0.36	−6.07 ± 0.31	>0.05	>0.05	>0.05
9 mm	−5.92 ± 0.25	−5.92 ± 0.37	−5.95 ± 0.37	>0.05	>0.05	>0.05
Percentage of variation of posterior curvature						
2 mm	6.00 ± 10.76	11.28 ± 13.35	7.96 ± 12.88	>0.05	>0.05	>0.05
3 mm	−0.88 ± 1.39	−1.52 ± 1.87	−4.45 ± 2.66	>0.05	**0.032**	**<0.05**
4 mm	−0.90 ± 1.02	−1.61 ± 1.61	−5.39 ± 2.79	>0.05	**<0.001**	**<0.001**
5 mm	−1.06 ± 0.88	−1.73 ± 1.31	−5.57 ± 2.88	>0.05	**<0.0001**	**<0.0001**
6 mm	−1.33 ± 0.94	−1.88 ± 1.02	−5.32 ± 2.88	>0.05	**<0.0001**	**<0.0001**
7 mm	−1.56 ± 1.11	−1.55 ± 1.99	−4.64 ± 2.73	>0.05	**<0.0001**	**<0.0001**
8 mm	−1.66 ± 1.00	−1.06 ± 2.21	−3.19 ± 2.45	>0.05	**<0.0001**	**<0.0001**
9 mm	−1.85 ± 1.81	−1.91 ± 2.74	−2.00 ± 2.62	>0.05	**<0.0001**	**<0.0001**

P-values in bold denote statistically significant differences.

FI: irregularity at 3 and 5 mm

FA: all the studied indices

The discriminant functions can be used to predict the class of a new observation with unknown class.

Receiver operating characteristic (ROC) curves were plotted to obtain critical values that allow classification with maximum accuracy. For the output values of the discriminant functions tested, the area under the ROC curve (AUROC), sensitivity [true positive/(true positive+false negative)], specificity [true negative/(true negative+false positive)], accuracy [(true positive+true negative)/total number of cases], and cutoff value were calculated.

Results

Table 1 shows the demographic data in the three groups. There were significantly more men in the KC and the FFKC groups ($P < 0.001$). The mean age was not significantly different between the groups. In Table 2 the mean ± SD of the studied factors are shown as well as an intergroup comparison.

Normal and FFKC Groups

There was no significant difference between the normal group and the FFKC group for the ABFS, PBFS, SK_{max}, and SK_{min}. The 3- and 5-mm irregularities were significantly higher in the FFKC group. The CP was significantly lower in the FFKC group compared with that in the normal group, and the TP was significantly thinner and decentered. The differences between the CP and the TP (CP − TP) and the PETP were significantly larger in the FFKC group than in the normal group (Table 2). The MACE, MPCE, and AETP were not significantly different between the two groups.

Normal and KC Groups

The anterior and posterior elevation indices deriving from the Quad Map (ABFS, PBFS, SK_{max} and SK_{min}, irregularity at 3 and 5 mm) were significantly different in the KC group than in the normal group. The CP and the TP were also significantly different in the two groups and the difference between the CP and the TP (CP − TP) was significantly larger in the KC group. The TP was more inferotemporally located in the KC group than in the normal group, and the MACE, MPCE, AETP, and PETP were significantly higher in the KC group (Table 2).

Anterior Corneal Curvature

The mean anterior curvature was significantly different for any distance from the cornea's TP, except at 8.0 and 9.0 mm between the normal group and the KC group, but not between the normal group and the FFKC group (Table 2, Fig. 3). The cornea flattened significantly faster at 5.0, 6.0, and 7.0 mm from the TP in the FFKC group compared to the normal group (Fig. 4).

Corneal Thickness Spatial Profile

The mean thickness of all corneal zones was significantly lower in the FFKC and KC group compared to the normal group (Table 2, Fig. 5). The cornea thickened significantly faster from the TP to the periphery in all corneal zones in the FFKC and KC group compared to the normal group (Fig. 6).

Posterior Corneal Curvature

The mean posterior curvature was significantly lower from a 1- to 6-mm distance from the cornea's TP between the normal group and the KC group, but not between the normal group and the FFKC group (Table 2). The cornea flattened signifi-

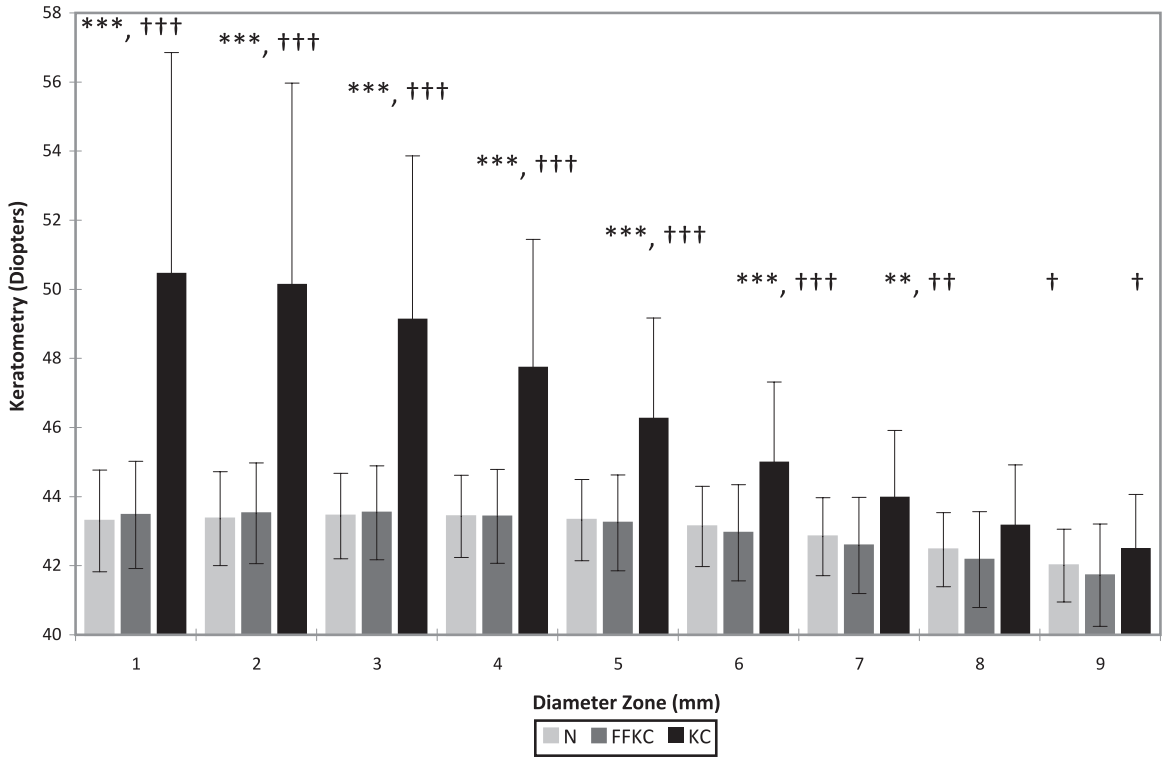

Figure 3. Mean corneal curvatures on rings concentric to the TP. ***$P < 0.0001$ between the N and KC groups; **$P < 0.001$ between the N and KC groups; †††$P < 0.0001$ between the FFKC and KC groups; ††$P < 0.001$ between the FFKC and KC groups; †$P < 0.05$ between the FFKC and KC groups.

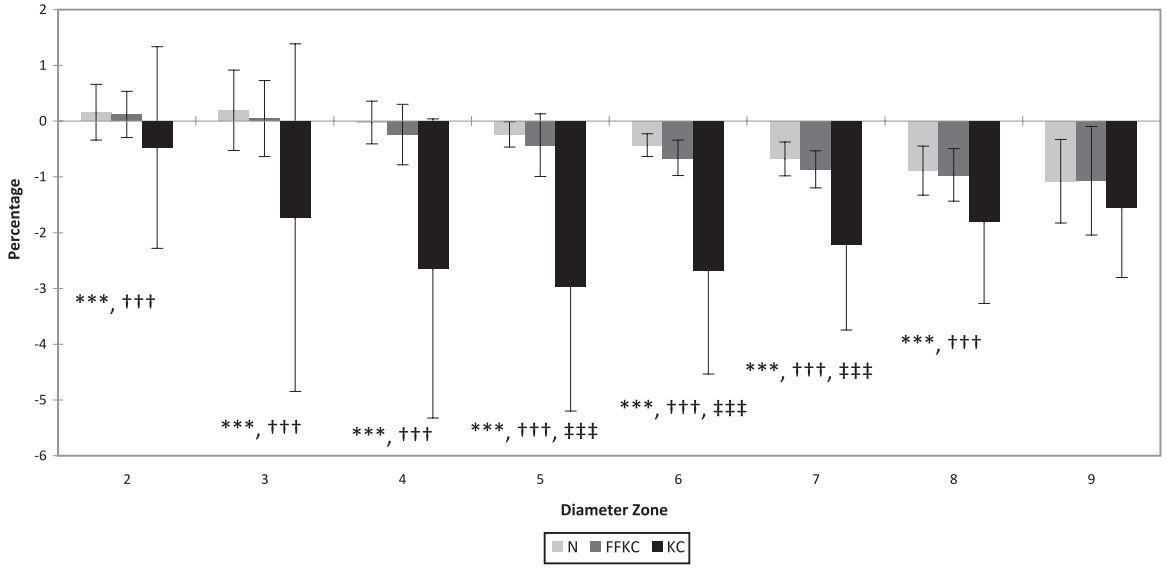

FIGURE 4. Percentage of variation of anterior curvature from the TP to the periphery. ***$P < 0.0001$ between the N and KC groups; †††$P < 0.0001$ between the FFKC and KC groups; ‡‡‡$P < 0.0001$ between the N and FFKC groups.

cantly faster from 3.0 to 9.0 mm from the TP in the KC group compared to the normal group (Table 2).

Discriminant Analysis and ROC Curve

The formulas for all discriminant functions are shown in the Appendix. The functions were derived from N and FFKC indices and their output values were tested to differentiate between the N and FFKC groups and the N and KC groups. The output values of the discriminant function were significantly different between the three groups ($P < 0.0001$; Table 3).

The function FT consisted of the TP, the difference between the CP and TP, the decentration of the TP, and the AETP and PETP, where the difference between the CP and TP had the highest discriminant coefficient (0.501).

The function FPTI consisted of the PTI over the entire cornea, where the PTI at 4 mm from the TP had the highest discriminant coefficient (2.846).

The function FPVAK consisted of the PVAK over the entire cornea, where the PVAK at 5 mm from the TP had the highest discriminant coefficient (1.019).

The function FPVPK consisted of the PVPK over the entire cornea, where the PVPK at 2 mm from the TP had the highest discriminant coefficient (0.527).

The function FI consisted of the irregularity at 3 and 5 mm, where the irregularity at 5 mm had the highest discriminant coefficient (0.543).

The function FA was derived from all the studied factors. The PTI at 5 and 6 mm from the TP had the highest relative

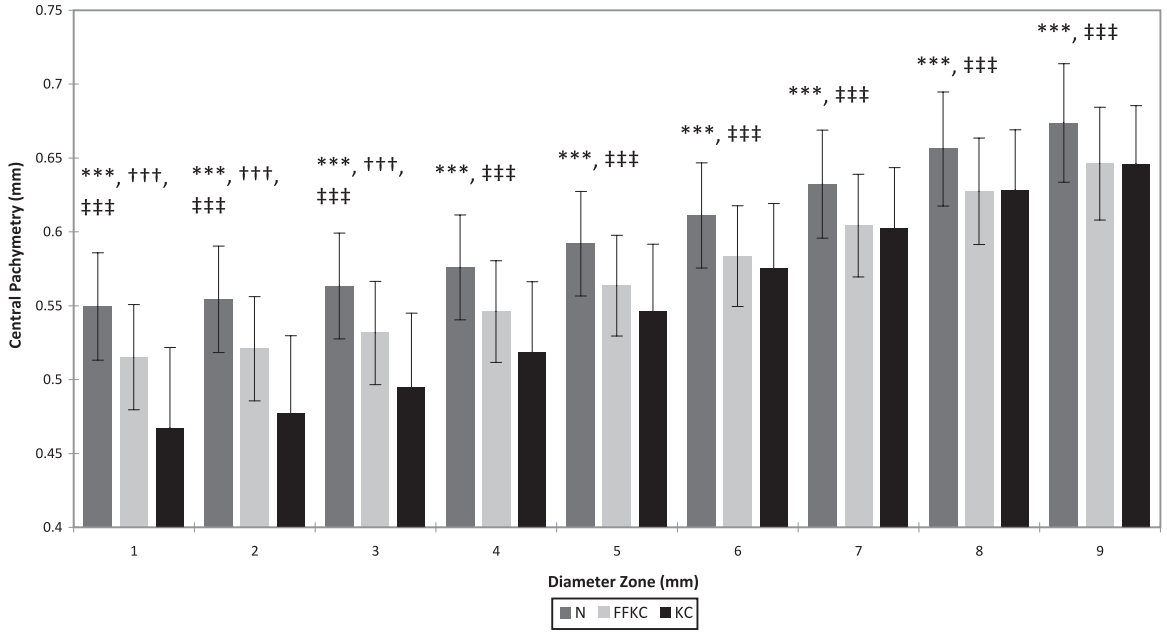

FIGURE 5. Mean corneal thicknesses on concentric rings to the TP. ***$P < 0.0001$ between the N and KC groups; †††$P < 0.0001$ between the FFKC and KC groups; ‡‡‡$P < 0.0001$ between the N and FFKC groups.

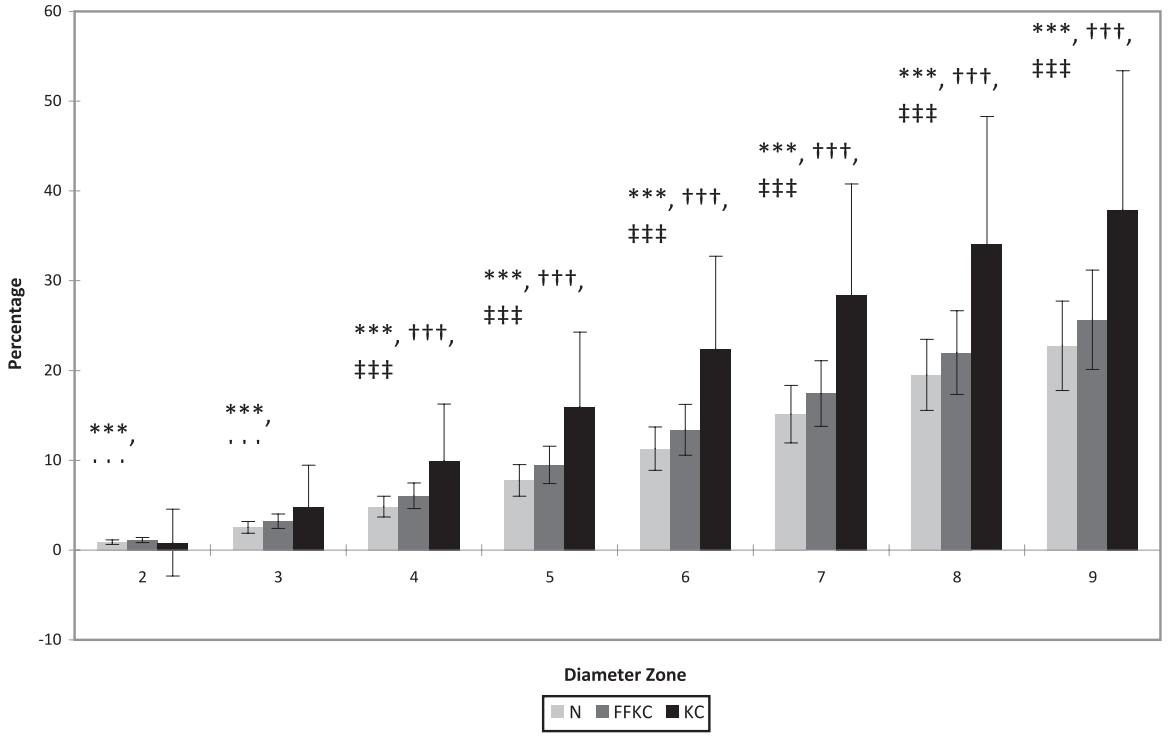

FIGURE 6. Percentage increase in thickness from the TP to the periphery. ***$P < 0.0001$ between the N and KC groups; †††$P < 0.0001$ between the FFKC and KC groups; ‡‡‡$P < 0.0001$ between the N and FFKC groups.

discriminant coefficient (6.555 and 5.826, respectively) followed by the PTIs at 3 (3.117), 8 (1.497), and 2 (1.473) mm; the MPCE (1.384); the PVAK at 5 mm (1.203); and the PVPK at 4 mm (1.040). Others indices had a relative discriminant coefficient less than 1.

For the distinction between the N group and the FFKC, the FA based on all the studied indices reached an AUROC of 0.98, a sensitivity of 93%, a specificity of 92%, and an accuracy of 92% (Table 4). The other functions had an accuracy between 71% (FPVAK) and 76% (FT).

For the distinction between the N and the KC groups, all the output values of the discriminant functions yielded a sensitivity and a specificity higher than 90% except the FPVPK (87% for both), with the FI reaching the same accuracy as FA (99%; Table 4). The FA could differentiate the KC group from the N group with an AUROC of 0.99, a sensitivity of 97%, a specificity of 100%, and an accuracy of 99%. In Figures 7 and 8, the ROC curves of all the discriminant functions are displayed graphically.

TABLE 3. The Output Values of the Discriminant Functions

	N	FFKC	KC
FA	0.55 ± 0.78	3.55 ± 1.32	14.73 ± 8.60
	−0.67 to 2.28	1.66 to 6.33	2.14 to 31.99
FT	7.04 ± 0.77	5.35 ± 1.31	1.35 ± 3.27
	5.44 to 8.37	1.76 to 7.72	−5.45 to 7.43
FPTI	2.88 ± 0.91	3.99 ± 1.13	7.65 ± 3.47
	0.54 to 4.94	2.05 to 7.45	1.89 to 16.19
FPVAK	1.89 ± 0.82	2.35 ± 1.26	10.30 ± 7.55
	−0.31 to 3.64	−0.25 to 5.20	−10.64 to 25.62
FPVPK	0.57 ± 0.91	1.63 ± 1.13	3.70 ± 2.45
	−1.49 to 4.37	−0.28 to 4.05	−0.40 to 10.34
FI	3.72 ± 0.89	4.76 ± 1.16	15.13 ± 7.16
	2.37 to 7.00	3.22 to 8.26	6.25 to 29.00

The data are expressed as the mean, standard deviation, and range ($P < 0.001$ between the three groups).

DISCUSSION

To describe the characteristics of the earliest form of KC and avoid any biases in the training sample, it is crucial that the selection of patients in each studied group be objective. For that reason, the artificial intelligence of the NCN is preponderant and, while others studied clinically unilateral KC,[8,23,35] ours is the first study to our knowledge, to describe characteristics of FFKC selected using neural network criteria: a positive percentage of similarity to normal eyes on the NCN with a null percentage of similarity to KC and KCS. KC is defined as a condition in which the cornea assumes a conical shape because of thinning and protrusion.[22] We recently described a case of bilateral postfemtosecond LASIK ectasia occurring in topographically normal eyes presenting only a 20-μm difference in the CP and in the TP between both eyes,[36] and Li Lim et al.[35] and Pflugfelder et al.[37] have shown that corneal thinning is a key pathologic feature of KC. Thus, studying the characteristics of the cornea centered on the TP, which corresponds to the most affected point, can be of valuable interest, and the preliminary work of Ambrosio et al.[33] showed consistent results and proved that the percentage of thickness increase from the TP to the periphery is different in KC eyes compared to normal eyes. Our results went further and provided evidence that the PTI in the mildest manifestation of the keratoconus disease (FFKC) is already higher compared to normal eyes (Fig. 6). The PVAK was also significantly different at a 5.0-, 6.0-, and 7.0-mm distance from the TP between normal eyes and FFKC eyes (Fig. 4). These results strongly suggest that the mildest form of KC is characterized by a quick modification of the cornea's shape and thickness from the TP to the periphery.

There was no significant difference in the ABFS, PBFS, SK_{max}, and SK_{min} between normal eyes and FFKC (Table 2), which reflected the null similarity to KCS found on the NCN.

TABLE 4. Data of the Discriminant Functions

Discriminant Function	Cutoff Value		AUROC		Sensitivity (%)		Specificity (%)		Accuracy (%)	
	N vs. FFKC	N vs. KC	N vs. FFKC	N vs. KC	N vs. FFKC	N vs. KC	N vs. FFKC	N vs. KC	N vs. FFKC	N vs. KC
FA	≥1.55	≥2.69	0.98	0.99	93	97	92	100	92	99
FT	≤6.66	≤5.71	0.86	0.97	85	93	71	93	76	93
FPTI	≥3.38	≥4.18	0.77	0.93	70	90	72	93	72	92
FPVAK	≥1.75	≥3.36	0.74	0.94	70	90	71	97	71	95
FPVPK	≥0.88	≥1.31	0.78	0.91	72	87	71	87	72	87
FI	≥4.13	≥6.25	0.78	0.99	72	100	71	99	72	99

One of the first detectable signs of keratoconus with Placido corneal topography is a localized steepening.[15] The FFKC is the mildest stage of the disease; the eyes included in our FFKC group were negative for KC and KCS detection, on the basis of anterior curvature data only. Thus, current Placido-based indices were not sensitive enough to detect the earliest forms of KC. Irregularity indices at 3 and 5 mm show the optical surface irregularity that is proportional to the standard deviation of the axis-independent surface curvature. They are calculated automatically from within the Orbscan IIz software, according to a statistical combination of the standard deviations of the mean and toric curvatures.[38] Some investigators have reported that these irregularity indices were significantly higher in KCS corneas than in normal corneas.[35,39] Of interest, in our study, the 3- and 5-mm irregularity indices were significantly higher in FFKC than in normal corneas; however, this level of irregularity was not sufficient to exceed the threshold for positive KCS suspicion with the NCN. The CP and the TP were significantly lower in FFKC ($P < 0.0001$, Table 2), and the subtraction of the CP from the TP (CP − TP) significantly differentiated the three groups (Table 2). It had been reported that the TP of keratoconic eyes is typically located inferotemporally.[40,41] We found that the TP of the FFKCs was located inferiorly compared with that of the normal eyes ($P < 0.0001$, Table 2). Horizontal and vertical displacement of the TP on the pachymetry map is commonly associated with poor patient fixation or operator centration during acquisition of the Orbscan IIz image.[6] However, multiple Orbscan images were acquired for our FFKC groups. Many studies described modifications in the posterior corneal surface in keratoconus,[14,35,42] and some investigators have proposed a KC screening algorithm, using the posterior elevation on Orbscan IIz combined with videokeratography.[9]The PETP was significantly higher in FFKC ($P < 0.0001$, Table 2) compared with normal corneas. Thus, even if not identified as suspect by Placido topography indices, the FFKC group had PETP significantly higher than in the normal corneas. This result corroborates the hypothesis that an increase in posterior elevation concomitant to paracentral corneal thinning may be the first sign of subclinical keratoconus.[9,14]

Tomidokoro et al.[43] showed that the central posterior corneal curvature is significantly lower (larger absolute value) in KCS and KC eyes than in normal eyes and concluded that deformation, including local protrusion, occurs not only in the anterior but also in the posterior corneal surface of keratoconus eyes. We found a significantly larger absolute value for posterior curvature from a 1.0- to 6.0-mm distance from the TP in KC eyes compared to the N eyes; however, the difference was not significantly different between the N and FFKC groups. The PVPK from the TP was not significantly different between the N and FFKC groups. Thus, elevation indices of the posterior surface (MPCE, PETP) seem to be more sensitive than posterior curvature indices in discriminating between normal eyes and mild KC eyes.

As shown in Table 4, most of the discriminant functions were able to separate between the N and the KC group which supports the idea that frank KC is an easily detectable entity.

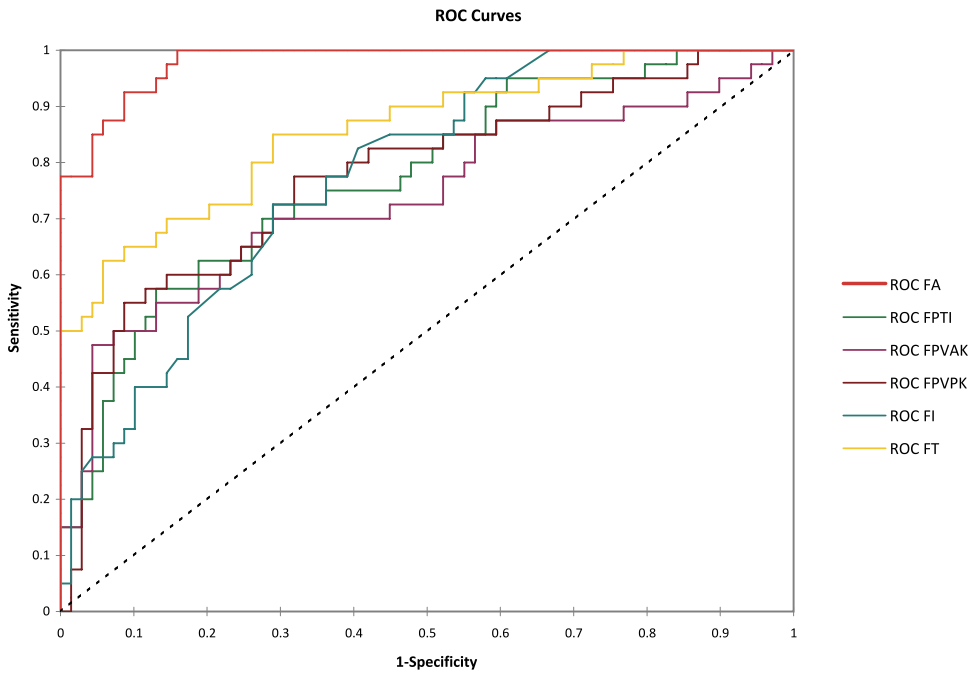

FIGURE 7. ROCs of the different functions for discrimination between the N and FFKC groups.

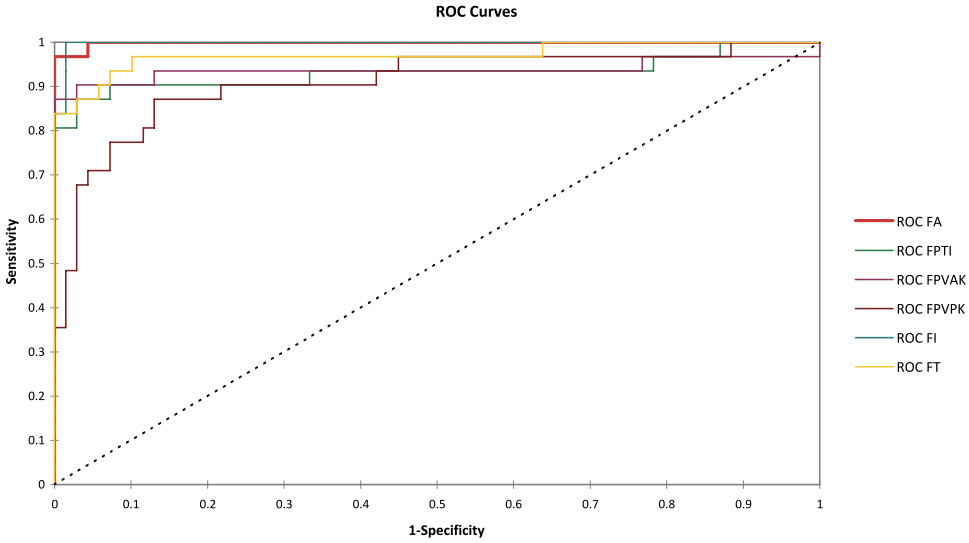

FIGURE 8. ROCs of the different functions for discrimination between the N and KC groups.

Furthermore, combining the anterior surface irregularity indices only provides a highly accurate tool in detecting KC (FI: sensitivity, 100%; specificity, 99%; and accuracy, 99%). This accuracy reached the one obtained with the association of all the studied factors (FA: sensitivity, 97%; specificity, 100%; and accuracy, 99%). However, all the functions that combine indices of the same origin (irregularity alone, TP-related indices alone, thickness spatial profile alone, or curvature alone; FI, FT, FPTI, FPVAK, and FPVPK) were not sufficiently accurate in separating the N group from the FFKC group (accuracy between 71% and 76%). Only the combination of all the studied indices in a discriminant function (FA) allowed the differentiation between the N group and the FFKC with a good accuracy (92%) (sensitivity, 92.5%; specificity, 92%). As the reported frequencies of unilateral KC range between 0.5% and 4%, cases of true unilateral KC may rarely occur, probably due to an intense trauma or severe eye rubbing. The low frequency of occurrence may explain the sensitivity of 92.5% in differentiating between the N and FFKC groups; the undetected cases (three false negative) may be true unilateral KC. Using the same function, differentiation between the N and KC groups is possible with a sensitivity of 97% and a specificity of 100% (Table 4). Discriminant functions are interpreted by means of standardized coefficients. The larger the standardized coefficient, the greater the contribution of the respective variable to the discrimination between groups. Spatial thickness profile indices and MPCE were the most important contributors to FA.

This study showed that indices generated from corneal thickness and curvature measurements over the entire cornea and calculations of the percentage of thickness increase and the percentage of anterior and posterior curvature variation from the TP to the periphery can identify very mild forms of KC that are not detected by Placido topography. However, we cannot conclude that any single parameter taken alone is sufficient to distinguish a normal from a suspect cornea, as the studied indices showed some degree of overlap in normal and pathologic corneas. A retrospective study of all the reported indices in cases of unsolved ectasia (without known risk factors such as KCS aspect or residual stromal bed of <300 μm) could confirm the link between our findings and the risk of ectasia. In addition, it could not be ruled out that there are other entities at risk for iatrogenic ectasia that could not be detected by our approach.

Currently, most diagnostic and classification criteria for keratoconus are based on anterior corneal curvature data[19,32,44] and do not take into account the spatial thickness profile and other corneal indices provided by tomography. We believe that evaluating those indices in conjunction with the parameters provided by Placido topography may help in creating artificial intelligence more sensitive and specific for the detection of corneas at risk for refractive surgery. Considering our results, new charts and graphs exploring data derived from elevation and pachymetry maps should be generalized in future corneal topography software to help the clinician in detecting mild ectasia.

References

1. Binder PS. Analysis of ectasia after laser in situ keratomileusis: risk factors. *J Cataract Refract Surg.* 2007;33:1530–1538.
2. Binder PS. Risk factors for ectasia after LASIK. *J Cataract Refract Surg.* 2008;34:2010–2011.
3. Randleman JB, Trattler WB, Stulting RD. Validation of the Ectasia Risk Score System for preoperative laser in situ keratomileusis screening. *Am J Ophthalmol.* 2008;145:813–818.
4. Randleman JB, Woodward M, Lynn MJ, Stulting RD. Risk assessment for ectasia after corneal refractive surgery. *Ophthalmology.* 2008;115:37–50.
5. Saad A, Lteif Y, Azan E, Gatinel D. Biomechanical properties of keratoconus suspect eyes. *Invest Ophthalmol Vis Sci.* 2010:51:2912–2916.
6. Nilforoushan MR, Speaker M, Marmor M, et al. Comparative evaluation of refractive surgery candidates with Placido topography, Orbscan II, Pentacam, and wavefront analysis. *J Cataract Refract Surg.* 2008;34:623–631.
7. Li X, Yang H, Rabinowitz YS. Keratoconus: classification scheme based on videokeratography and clinical signs. *J Cataract Refract Surg.* 2009;35:1597–1603.
8. Shirayama-Suzuki M, Amano S, Honda N, Usui T, Yamagami S, Oshika T. Longitudinal analysis of corneal topography in suspected keratoconus. *Br J Ophthalmol.* 2009;93:815–819.
9. Rao SN, Raviv T, Majmudar PA, Epstein RJ. Role of Orbscan II in screening keratoconus suspects before refractive corneal surgery. *Ophthalmology.* 2002;109:1642–1646.
10. Schweitzer C, Roberts CJ, Mahmoud AM, Colin J, Maurice-Tison S, Kerautret J. Screening of forme fruste keratoconus with the ocular response analyzer. *Invest Ophthalmol Vis Sci.* 2010;51:2403–2410.
11. Buhren J, Kuhne C, Kohnen T. Wavefront analysis for the diagnosis of subclinical keratoconus (in German). *Ophthalmologe.* 2006; 103:783–790.
12. Buhren J, Kuhne C, Kohnen T. Defining subclinical keratoconus using corneal first-surface higher-order aberrations. *Am J Ophthalmol.* 2007;143:381–389.
13. Seiler T, Quurke AW. Iatrogenic keratectasia after LASIK in a case of forme fruste keratoconus. *J Cataract Refract Surg.* 1998;24: 1007–1009.

14. Schlegel Z, Hoang-xuan T, Gatinel D. Comparison of and correlation between anterior and posterior corneal elevation maps in normal eyes and keratoconus-suspect eyes. *J Cataract Refract Surg.* 2008;34:789–795.
15. Klyce SD. Chasing the suspect: keratoconus. *Br J Ophthalmol.* 2009;93:845–847.
16. Klyce SD, Smolek MK, Maeda N. Keratoconus detection with the KISA% method-another view. *J Cataract Refract Surg.* 2000;26:472–474.
17. Rabinowitz YS, McDonnell PJ. Computer-assisted corneal topography in keratoconus. *Refract Corneal Surg.* 1989;5:400–408.
18. Rabinowitz YS, Nesburn AB, McDonnell PJ. Videokeratography of the fellow eye in unilateral keratoconus. *Ophthalmology.* 1993; 100:181–186.
19. Rabinowitz YS, Rasheed K. KISA% index: a quantitative videokeratography algorithm embodying minimal topographic criteria for diagnosing keratoconus. *J Cataract Refract Surg.* 1999;25:1327–1335.
20. Mahon L, Kent D. Can true monocular keratoconus occur? *Clin Exp Optom.* 2004;87:126, author reply 126.
21. Kennedy RH, Bourne WM, Dyer JA. A 48-year clinical and epidemiologic study of keratoconus. *Am J Ophthalmol.* 1986;101:267–273.
22. Krachmer JH, Feder RS, Belin MW. Keratoconus and related noninflammatory corneal thinning disorders. *Surv Ophthalmol.* 1984; 28:293–322.
23. Li x, Rabinowitz YS, Rasheed K, Yang H. Longitudinal study of the normal eyes in unilateral keratoconus patients. *Ophthalmology.* 2004;111:440–446.
24. Holland DR, Maeda N, Hannush SB, et al. Unilateral keratoconus. Incidence and quantitative topographic analysis. *Ophthalmology.* 1997;104:1409–1413.
25. Ihalainen A. Clinical and epidemiological features of keratoconus genetic and external factors in the pathogenesis of the disease. *Acta Ophthalmol Suppl.* 1986;178:1–64.
26. Jacobs DS, Dohlman CH. Is keratoconus genetic? *Int Ophthalmol Clin.* 1993;33:249–260.
27. Rabinowitz YS, Maumenee IH, Lundergan MK, et al. Molecular genetic analysis in autosomal dominant keratoconus. *Cornea.* 1992;11:302–308.
28. Armitage JA, Bruce AS, Phillips AJ, Lindsay RG. Morphological variants in keratoconus: anatomical observation or aetiologically significant? *Aust N Z J Ophthalmol.* 1998;26(suppl 1):S68–S70.
29. Amsler M. The "forme fruste" of keratoconus (in German). *Wien Klin Wochenschr.* 1961;73:842–843.
30. Buscemi PM. Nidek corneal navigator software for topographic analysis of corneal states. *J Refract Surg.* 2004;20:S747–S750.
31. Klyce SD, Karon MD, Smolek MK. Screening patients with the corneal navigator. *J Refract Surg.* 2005;21:S617–S622.
32. Maeda N, Klyce SD, Smolek MK. Neural network classification of corneal topography: preliminary demonstration. *Invest Ophthalmol Vis Sci.* 1995;36:1327–1335.
33. Ambrosio R Jr, Alonso RS, Luz A, Coca Velarde LG. Corneal-thickness spatial profile and corneal-volume distribution: tomographic indices to detect keratoconus. *J Cataract Refract Surg.* 2006;32:1851–1859.
34. Luz A, Ursulio M, Castaneda D, Ambrosio R, Jr. Corneal thickness progression from the thinnest point to the limbus: study based on a normal and a keratoconus population to create reference values (in Portuguese). *Arq Bras Oftalmol.* 2006;69:579–583.
35. Lim L, Wei RH, Chan WK, Tan DT. Evaluation of keratoconus in Asians: role of Orbscan II and Tomey TMS-2 corneal topography. *Am J Ophthalmol.* 2007;143:390–400.
36. Saad A, Gatinel D. Bilateral corneal ectasia after laser in situ keratomileusis in patient with isolated difference in central corneal thickness between eyes. *J Cataract Refract Surg.* 36: 1033–1035.
37. Pflugfelder SC, Liu Z, Feuer W, Verm A. Corneal thickness indices discriminate between keratoconus and contact lens-induced corneal thinning. *Ophthalmology.* 2002;109:2336–2341.
38. Sonmez B, Doan MP, Hamilton DR. Identification of scanning slit-beam topographic parameters important in distinguishing normal from keratoconic corneal morphologic features. *Am J Ophthalmol.* 2007;143:401–408.
39. Tanabe T, Tomidokoro A, Samejima T, et al. Corneal regular and irregular astigmatism assessed by Fourier analysis of videokeratography data in normal and pathologic eyes. *Ophthalmology.* 2004; 111:752–757.
40. Levy D, Hutchings H, Rouland JF, et al. Videokeratographic anomalies in familial keratoconus. *Ophthalmology.* 2004;111:867–874.
41. Rabinowitz YS, Rasheed K, Yang H, Elashoff J. Accuracy of ultrasonic pachymetry and videokeratography in detecting keratoconus. *J Cataract Refract Surg.* 1998;24:196–201.
42. Auffarth GU, Wang L, Volcker HE. Keratoconus evaluation using the Orbscan Topography System. *J Cataract Refract Surg.* 2000; 26:222–228.
43. Tomidokoro A, Oshika T, Amano S, Higaki S, Maeda N, Miyata K. Changes in anterior and posterior corneal curvatures in keratoconus. *Ophthalmology.* 2000;107:1328–1332.
44. Rabinowitz YS. Keratoconus. *Surv Ophthalmol.* 1998;42:297–319.

APPENDIX

Relative Coefficients of the Discriminant Function Indices

FT $0.412 \times TP - 0.501 \times (CP - TP) - 0.188 \times DTP - 0.362 \times AETP + 0.220 \times PETP$

FPTI $-0.062 \times PTI2 - 1.468 \times PTI3 + 2.846 \times PTI4 + 1.436 \times PTI5 - 1.0 \times PTI6 - 1.203 \times PTI7 - 0.868 \times PTI8 + 1.219 \times PTI9$

FPVAK $-0.027 \times PVAK2 + 0.463 \times PVAK3 - 0.824 \times PVAK4 + 0.522 \times PVAK5 - 1.019 \times PVAK6 + 0.013 \times PVAK7 - 0.075 \times PVAK8 + 0.236 \times PVAK9$

FPVPK $0.527 \times PVPK2 - 0.195 \times PVPK3 + 0.016 \times PVPK4 - 0.518 \times PVPK5 - 0.258 \times PVPK6 + 0.090 \times PVPK7 + 0.482 \times PVPK8 + 0.029 \times PVPK9$

FI $0.322 \times (Irreg\ 3\ mm) + 0.543 \times (Irreg\ 5\ mm)$

FA $0.174 \times (Irreg\ 3\ mm) + 0.151 \times (Irreg\ 5\ mm) - 0.180 \times (TP) + 0.065 \times (CP - TP) - 0.685 \times dec\ IyI + 0.547 \times (DTP) - 0.780 \times (MACE) + 1.384 \times (MPCE) + 0.635 \times (AETP) - 0.782 \times (PETP) + 1.473 \times (PTI2) - 3.117 \times (PTI3) + 0.841 \times (PTI4) + 6.555 \times (PTI5) - 5.826 \times (PTI6) - 1.198 \times (PTI7) + 1.497 \times (PTI8) + 0.179 \times (PTI9) + 0.433 \times (PVAK2) - 0.349 \times (PVAK3) - 0.854 \times (PVAK4) + 1.203 \times (PVAK5) - 0.979 \times (PVAK6) + 0.250 \times (PVAK7) + 0.324 \times (PVAK8) + 0.217 \times (PVAK9) + 0.650 \times (PVPK2) - 0.290 \times (PVPK3) + 1.040 \times (PVPK4) - 0.736 \times (PVPK5) + 0.604 \times (PVPK6) + 0.449 \times (PVPK7) + 0.522 \times (PVPK8) - 0.340 \times (PVPK9)$